Summer 2016

Deterministic simulation of thermal neutron radiography and tomography

Rajarshi Pal Chowdhury

Department:

DETERMINISTIC SIMULATION OF THERMAL NEUTRON RADIOGRAPHY AND TOMOGRAPHY

by

RAJARSHI PAL CHOWDHURY

A THESIS

Presented to the Faculty of the Graduate School of the

MISSOURI UNIVERSITY OF SCIENCE AND TECHNOLOGY

In Partial Fulfillment of the Requirements for the Degree

MASTER OF SCIENCE

in

NUCLEAR ENGINEERING

2016

Approved by:

Xin Liu, Advisor

Hyoung Koo Lee

Ayodeji Alajo

ABSTRACT

In recent years, thermal neutron radiography and tomography have gained much attention as one of the nondestructive testing methods. However, the application of thermal neutron radiography and tomography hindered by their technical complexity, radiation shielding, and time-consuming data collection processes. Monte Carlo simulations have been developed in the past to improve the neutron imaging facility's ability. In this present work, a new deterministic simulation approach has been proposed and demonstrated to simulate neutron radiographs numerically using a ray tracing algorithm. This approach has made the simulation of neutron radiographs much faster than by previously used stochastic methods (i.e Monte Carlo methods). The major problem with neutron radiography and tomography simulation is finding a suitable scatter model. In this paper, an analytic scatter model has been proposed that is validated by a Monte Carlo simulation. Two simulation geometries have been analyzed in this work. One is a highly scattering medium, another is medium scattering media. It has been shown that this algorithm works well in the medium scattering media. The scatter model has been verified using Monte Carlo method (MCNP5).There are some empirical parameters that have been determined using curve fitting methods using MATLAB. There are some disadvantages of using the scatter correction algorithm proposed in this work, but the advantages are far more rewarding. This method of simulation reduces the time of simulation in 5-10 seconds compared to several hours using Monte Carlo methods and can be used for rapid prototyping for neutron imaging facilities. Filtered back-projection with a ramp filter has been used for reconstruction.

ACKNOWLEDGEMENTS

I thank my advisor Dr.Xin Liu for giving me valuable guidance and required funding to work on my masters project. I also like to thank my colleagues Edward Norris, Huseyin Sahiner and Zhongmin Jin for their valuable inputs and supports. I will also like to thank Dr. Ayodeji Alajo for helping me to solve some issues in MCNP. I will also like to thank Dr. Hyoung Koo Lee for giving me his valuable time to serve as one of the members in my thesis advisory committee. This work is supported by the U.S.Nuclear Regulatory Commission (NRC) Faculty Development Grant under Grant no. NRC-HQ-12-G-38-0039.

Finally I would like to thank my parents, my sister, my brother in-law, and my cute little niece Sreyoshi for their continuous support and encouragement. I would not be able to finish my work without them.

TABLE OF CONTENTS

Page

LIST OF ILLUSTRATIONS

LIST OF TABLES

1. INTRODUCTION

1.1. MOTIVATION

Neutron radiography is a well-established method of non-destructive testing (NDT) which has been there since 1950's [1]. In the last few years, neutron imaging has gained much more attention over other methods of imaging. Neutron interacts with materials in a complementary way compared to the X-ray imaging. The materials with high atomic numbers are opaque in X-ray imaging, compared to the neutron. This mode of imaging is preferred in the areas where it is needed to locate a material of low atomic number inside of a material with high atomic number. In many fields of research and industry it is important to locate moisture, crack, bubble flow, etc., inside a system. For example, in the field of archeology, it is sometimes important to determine the content of ancient sculptures [2], thermal neutron imaging is a core part of studies involving water content determination [3]. In nuclear engineering, neutron radiography and tomography is widely used for the inspection of fuel cells and neutron radiography is also used in thermal hydraulics to determine void fraction in pipes [4-5]. Thermal neutrons have high capability to distinguish between different materials as the thermal neutron cross sections are significantly different from low atomic number materials to high atomic number materials and even from one isotope to another. The attenuation probabilities of materials in case of thermal neutrons are not dependent on their atomic numbers. This property of thermal neutrons makes them suitable in non-destructive testing. So far the techniques that have been used for simulating neutron radiography are stochastic methods, such as Monte Carlo methods [6].

Simulating a neutron imaging facility's performance is of utmost importance. Simulating the images shows whether the imaging set up works efficiently or not. Based on the results of imaging facility, suitable and faster method needs to be developed. Monte Carlo methods need both significant time and resources to solve neutron imaging problem. To make neutron radiography more effective a faster method needs to be implemented. In this study, a deterministic method has been implemented to simulate thermal neutron radiography which is significantly faster than previously used methods. There is one disadvantage of using thermal neutrons as a mean to image hydrogenous materials such as, water, or any such biological sample. Hydrogen acts as a highly scattering medium in case of thermal neutrons. In case of imaging, scattered neutrons can degrade the quality of the image and introduce effect such as blurring of image at sharp edges. Scattering adds a neutron distribution to the detected signal, which makes the reconstruction procedure very challenging. So, before reconstruction of images, the effect of scatter needs to be removed or minimized without affecting signal quality. Therefore, a suitable scatter removal algorithm needs to be developed. The scatter correction methods available till date uses Monte Carlo methods such as MCNP to simulate the scatter effect. In case of neutron imaging MCNP takes a huge time to run. For example, in the geometry of this present study, it takes almost 10 hours to simulate a single radiograph using 5 million particle histories. Moreover, the same geometry needs to be simulated twice, once with scatter, and once without scatter. This makes the scatter correction algorithm not viable for practical purposes.

1.2. CHARACTERISTICS OF NEUTRONS

As a fundamental particle, neutron has the ability to provide a stream of unique characteristics which are proved to be essential in the imaging community. In this section, those attributes of neutrons are discussed. These properties of neutrons interacting with matter give underlying ideas of neutron imaging. As one of the main components of an atom, neutron was discovered in 1932 by J. Chadwick [7]. Neutron is electrically neutral, which makes it an attractive both in scattering and imaging applications. It interacts primarily with nuclei because of its charge neutrality; it is highly penetrating and is suitable enough to penetrate materials with higher atomic mass. These properties make neutrons suitable for imaging light materials, or investigating the inside of a large assembly in a non-destructive way. Another important fundamental property of neutron is its mass, ($m_n = 1.6749 \times 10^{-27} Kg$), which gives the neutron a de Broglie wavelength compared to the atomic distances in room temperatures (thermal energy range). The de Broglie wavelength, λ in units of nm, is given by

$$\lambda = \frac{h}{m_n v} = 395.6/v \quad (1)$$

Where, $h = 6.6261 \times 10^{-34} J - s$ is the Planck's constant and v is the neutron velocity in ms^{-1}.The neutron energy is given by:

$$E = \frac{1}{2} m_n v^2 = 5.2770 \times 10^{-6} v^2 \quad (2)$$

A neutron in thermal energy (room temperature 300K) will have a velocity of approximately 2224 ms^{-1} and corresponding wavelength of 0.18nm. Neutrons are typically produced either in reactors via the nuclear fission or in spallation neutron sources (where a high energy proton beam is incident on a heavy metal and produces neutrons).

These neutrons are in fast energy range (see Table 1.1). Thermal neutrons are more suitable for imaging purpose because they are easier to be detected than fast neutrons. The neutrons need to be slowed or cooled down. Moderators are used to convert fast neutrons to thermal or cold energy range. Generally hydrogen or hydrogenous materials, graphite, etc., are used for moderation.

Table 1.1. Neutron properties at various energy ranges.

Energy classification	Energy range (meV)	Velocity (ms^{-1})	Wavelength(nm)
Ultra-Cold	0.00025	6.9	57
Cold	1	437	0.9
Thermal	25	2187	0.18
Epithermal	1000	12,832	0.029

1.3. INTERACTIONS WITH MATTER AND CROSS SECTION

In thermal neutron imaging the principle lies in neutron interaction that attenuates a ray or beam of neutrons coming from a source. Neutrons can be removed from the incident beam by the object by two phenomena, absorption and scattering. Figure. 1.1. illustrates the attenuation of neutron beam incident perpendicularly on a thin sample of

thickness dx which is placed at a distance x from the source. The thickness is small enough so that it is only one atom layer thick and the neutrons can interact with all the atoms involved.

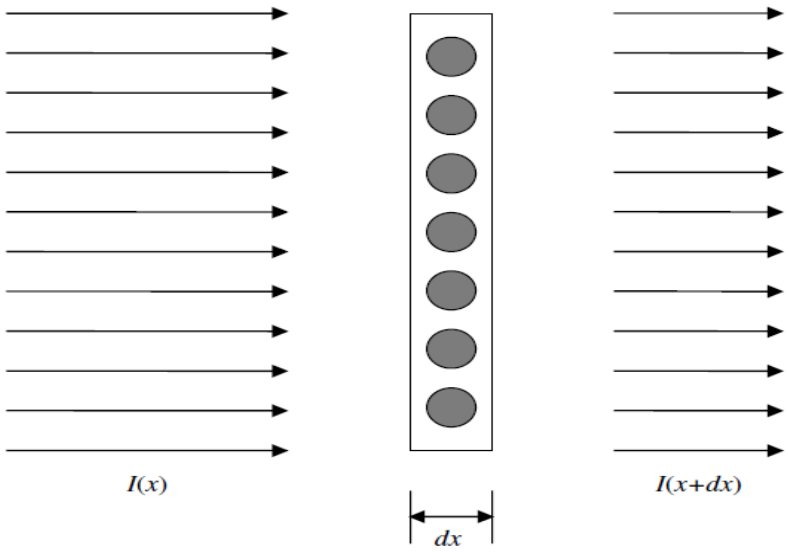

Figure. 1.1. Neutron interaction with matter.

Let $I(x)$ be the incident neutron flux, and $I(x + dx)$ be the transmitted flux. Let N be the number density of atoms in that layer. It is assumed that the atoms are particles of radius r. The neutron attenuation is given by the fractional area occupied by all the atoms in that layer, which is equal to $dx.N\pi r^2$. This gives:

$$I(x + dx) = I(x)(1 - dx.N\pi r^2) = I(x)(1 - dxN\sigma) \quad (3)$$

Where, σ is defined as the microscopic cross section. Microscopic cross section is defined as the effective interaction area between the neutron and the nucleus.

From Eq.3 the rate of change of I(x) is given by:

$$\frac{dI(x)}{dx} = -N\sigma I(x) \quad (4)$$

And the solution for $I(x)$ is given as below:

$$I(x) = I_0 \exp(-N\sigma x) \quad (5)$$

Where, I_0 is the incident neutron flux. The product $N\sigma$ is known as the macroscopic cross section. For an object with more than one material, the macroscopic cross section is the sum over all the macroscopic cross sections.

The neutron-nucleus interaction is of quantum mechanical in nature. Neutron interacts with an object either via absorption or scattering. The total microscopic cross section is given by

$$\sigma_t = \sigma_a + \sigma_s \quad (6)$$

Where, σ_a and σ_s are absorption and scattering cross section respectively. The neutron scattering cross section can be further divided into coherent and incoherent scattering. In coherent scattering, neutrons that are scattered primarily by different nuclei combine with one another to produce an interference pattern that depends on the relative locations of the atoms in the material. Incoherent scattering is the case when there are more than one isotope present in one sample. Neutrons interact with matter in five different ways.

(1) Elastic scattering

Neutron collides with the nucleus and loses its kinetic energy. Neutron loses more energy to heavier materials than to lighter materials. Elastic scattering is the most important phenomena to produce thermal or cold neutron from fast neutron sources.

(2) Inelastic scattering

Inelastic scattering is similar to elastic scattering but here when the neutron collides with the atomic nucleus it deposits part of its energy to the nucleus and takes it to an excited state. After collision, the nucleus emits gamma ray(s) to get back to the ground state. This type of scattering is not preferred in neutron radiography as it causes gamma emission which is considered as noise.

(3) Neutron capture

A neutron can be absorbed by the atomic nucleus to increase its atomic number by one. The new nucleus most likely becomes a radioactive nucleus and emits radiation.

(4) Charged particle emission

This phenomena is generally occurred by fast neutrons, where charged particles are emitted upon the incidence of neutrons.

(5) Fission

Fission occurs when upon incidence of a neutron, the nucleus divides into two nuclei and emit more than one neutrons in process.

In this present work, thermal neutrons are used as the source. Only the scattering and absorption phenomena is dominant in thermal neutron imaging. Elastic scattering is redominant in thermal neutron energy. The corresponding thermal neutron cross section of different materials (ranging from atomic number 1-100) is shown in Figure.1.2.

From Figure.1.2., it is clear that the scattering cross section and the absorption cross section does not have any linear relationship with the atomic number of the materials, and the scattering cross section is very high in case of lower atomic number materials such as hydrogen. Monochromatic energy source of energy 0.0253eV has been used as a source.

This is the most probable energy of a thermal neutron energy distribution. In this work, monochromatic energy source is used to ignore the effects of beam hardening. Thermal neutron energy distribution is a Watt distribution.

The velocity distribution function of thermal neutron energy range is given by the following equation:

$$\Phi(v)dv = \Phi\frac{2}{v_T^4}v^3\exp(-\left(\frac{v^2}{v_T^2}\right)) \quad (7)$$

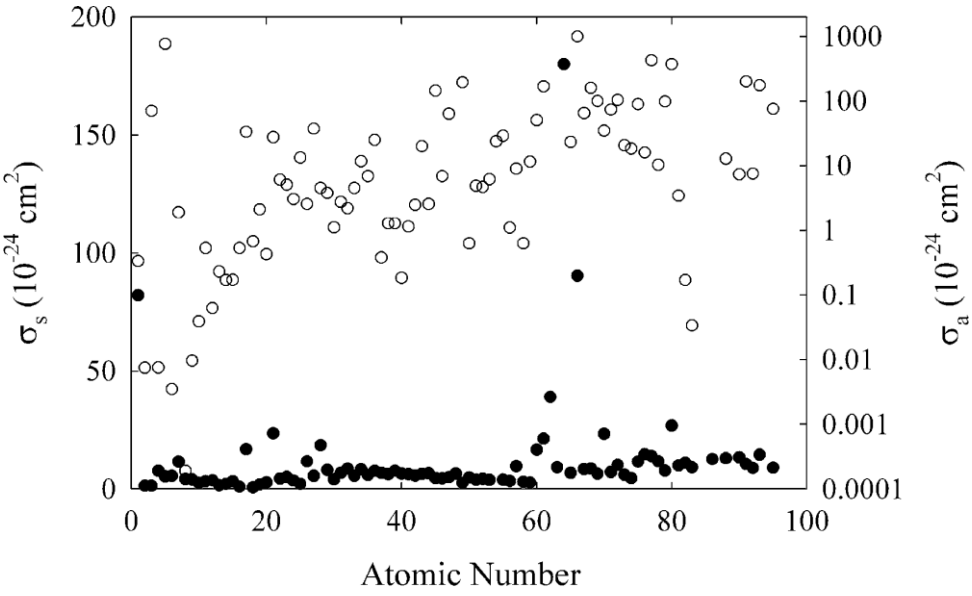

Figure.1.2. Thermal neutron scattering and absorption cross section distribution.

Where, $\Phi(v)$is the neutron velocity flux distribution, v is the neutron velocity and v_T is the neutron velocity at temperature equal to 293.6K ($\approx 2200m/s$). In this experiment, materials such as hydrogen, nitrogen, oxygen, calcium, iron, lead, etc., are used. The microscopic thermal neutron total and absorption cross sections are obtained from the neutron cross section library ENDF-B/VII.1 [23].There is no thermal neutron scattering cross section table available. For the imaging of above materials, the cross sections such as charged particle emission, fission are negligible and almost equal to zero.

1.4. PREVIOUS STUDIES ON NEUTRON IMAGING AND ITS SIMULATION

The idea of imaging is to create a contrast between different elements based on their inherent and unique properties like mass attenuation coefficients, conductivity, and microscopic cross sections. Neutron radiography uses the microscopic cross section property of materials to generate the radiograph. The main sources of image degradation in neutron radiography are scattering degradation, geometric degradation, displacement degradation, neutron spectral degradation and detector degradation. In neutron radiography the main mathematical equation can be expressed as

$$\frac{I}{I_0} = e^{-\Sigma_t(E).x} \tag{8}$$

Where, $\Sigma_t(E)$ is the total cross section of the material to be imaged. I and I_0 are the neutron intensity after and before incidence. The thickness of the material is defined as x. It is to be noted that the total material cross section is energy dependent. The scattering effect can be denoted by I_s. The main focus of this is to remove the scattering effect from the image. Scattering effect consists of neutrons scattering. The term point

scattered function has been introduced here. Equation 1 can be modified after eliminating the effects of scattered neutrons. The new equation can be represented as

$$\frac{I-I_s}{I_0} = \frac{\int_0^{E_0} \phi(E) e^{-\Sigma_t(E).x} dE}{\int_0^{E_0} \phi(E) dE} \quad (9)$$

ϕ is the neutron flux.The key focus of this work is to simulate the scattered neutrons using MCNP5 and find the probability distribution function (pdf) of these scattered neutrons using efficient analytical methods and subtract the pdf from the distribution of neutrons obtained from the original radiograph. The two key terms that has been discussed here are Point Spread function (PSF) and Point Scattered function (PscF). The point spread function is an image the system produces of a point like object. The PSF is the image plane response at an arbitrary point at the image axes when the flux coming from a point neutron source passes through an infinitesimally small hole of an neutron absorbing material. Ideally the PSFs are δ-functions.[25]

Another key term is the point scattered function (PScF) which has been discussed many times in this paper. It is defined as the density distribution of scattered neutrons on the detectors from a point source from which the neutrons incident on the target material directly. The PScF is dependent on the material thickness(x), distance from source to detectors (d) and the aperture angle of the source beam. So it can be said that the PScF is an integrated version of all the PSF at the image plane of the radiograph. When the Point Scattered Function is obtained it can be subtracted from the neutron distribution to remove the scattering degradation. There has been a lot of work in the area of neutron radiography using MCNP. Early important work was from Segal et al[8] when

they published their work regarding the calculation of point spread function of thermal neutron radiograph. The contribution of scattered neutron in the of the radiographed object was calculated using MCNP. But this work was insufficient as they failed to provide accurate distribution of dimensions and thickness. Murata et al [9] developed a method to to eliminate the effects of scattered neutrons from NR (Neutron radiography) by using a Cd grid. Raine et al [10] developed a correction algorithm using MCNP which determines the scattering contribution. But this work was limited only to high resolution with objects less than 2 centimeters in vertical or horizontal directions. Kardjilov et al (2005) [11] derived a procedure where they simulated the point scattered function for different position and thickness and property of target materials. Then they formulated a Gaussian function which fits the scattered neutron distribution of the target material at different distances from the source and different thickness of the material. Once the distribution of scattered neutrons was obtained in mathematical terms it was subtracted from the original radiograph to obtain scatter free image. The advantage of this work was once the distribution of scattered neutrons were obtained in terms of Gaussian distribution it eliminated the use of MCNP simulation each time a radiograph needs to be generated. Montaser Tharwat et al [6] devised a methodology using MCNP and MATLAB together for radiograph generation. The scattered neutron distribution was computed using MCNP and flux distribution of each pixel was determined individually which corresponds to the scattered neutrons and then a software tool named ImageJ from MATLAB was used to efficiently subtract this effect. LIU Shu-Quan et al [12] designed a method for scattering correction for fast neutrons at the NECTAR (Neutron Computerized Tomography And Radiography) facility at Germany. They calculated the

scattered fast neutron distribution at different distance and thickness using MCNP and subtracted it from original image to obtain scatter free image. The scattering distribution simulation took 10 hours with 64 CPUs parallel computing to obtain a PScF data with simulating 10^8 neutrons and with error less than 5%. The improvements that can be done from the previous works are first to find a method to run a huge number of particle history within a small amount of time. Generation of scattered neutron distribution using MCNP and subtraction is a time consuming procedure. If it needs to be implemented commercially a faster simulation method needs to be developed. The variance reduction methods in MCNP can be used to run the simulation very fast. The subtraction algorithm needs to be improved in such a way so that not only scattered neutron effects are eliminated other imaging irregularities should also be removed. An optimization between image quality and run time or particle history has to be analyzed so that a certain quality of image can be obtained with minimal cost.

When the image of an object is generated a spectrum of neutron energy is used. It can be analyzed which spectrum or range of energy gives the best resolution or image quality. It is also dependent on the thickness of the material and distance from the source and its material properties (cross section). So if some work is done as to which range provides minimum error it will more effective.

1.5. THERMAL NEUTRON RADIOGRAPHY AND TOMOGRAPHY

Thermal neutron radiography and tomography is a powerful tool of non-destructive imaging techniques. The images are formed due to attenuation of thermal neutron beam when it is propagated through the material to be visualized. Neutron radiography are in used since shortly after the discovery of neutrons by Chadwick in 1932[7]. Different

radioisotopes sources was used for neutron radiography [13]. Later accelerators and nuclear reactors were used as neutron source. Different types of position-sensitive detectors are implemented. Even with advanced instrumentation for radiography it lacked in one broad area which was all the information of a three dimensional object was restricted to two dimensional image. It was hard to distinguish between two materials with similar attenuation property. The issue was solved by the pioneer work of Hounsfield [14], who implemented computed tomography based on the early mathematical foundation provided by Radon in 1917[15].

1.5.1. Principles of Neutron Radiography. Radiography implements two-dimensional detection of transmitted neutron beam in a plane perpendicular to the direction of beam propagation (Figure.1.3). This creates a two-dimensional shadow of the object. The shadow or radiograph properties vary based on the thickness and integral attenuation properties of the material being imaged. The transmission T, is the ratio of the transmitted beam intensity I, and incident beam intensity I_0.

$$T = \frac{I}{I_0} \tag{10}$$

For any path along the transmission, according to the basic law of attenuation of radiation

$$I = I_0 \exp(-\int \mu ds\ ) \tag{11}$$

Where, μ is the local linear attenuation coefficient, and s is the propagation path. The attenuation co-efficient is a material property and is given by

$$\mu = \sigma \rho N_A / M \text{ or } \quad \mu = \sum_i \sigma_i\, \rho_i N_A / M_i \tag{12}$$

For single elements and for multiple elements respectively, where σ is the total interaction cross –section, ρ is the density of the material, N_A is the Avogadro's number, and M is the molar mass.

Neutrons passing through the object can interact with it in three ways: (1) absorption by the material, (2) scattering (coherent and incoherent) and (3) pass through the material without interaction (un-collided neutrons). In case of absorption the neutrons get lost or attenuated. In case of scattering, they slow down or change directions. Un-collided neutrons are the neutrons that reach the detector. Scattered neutrons also can reach the detector from a different direction and degrade image quality and create blur. In the present work, a method has been created to minimize the effect of scattering.

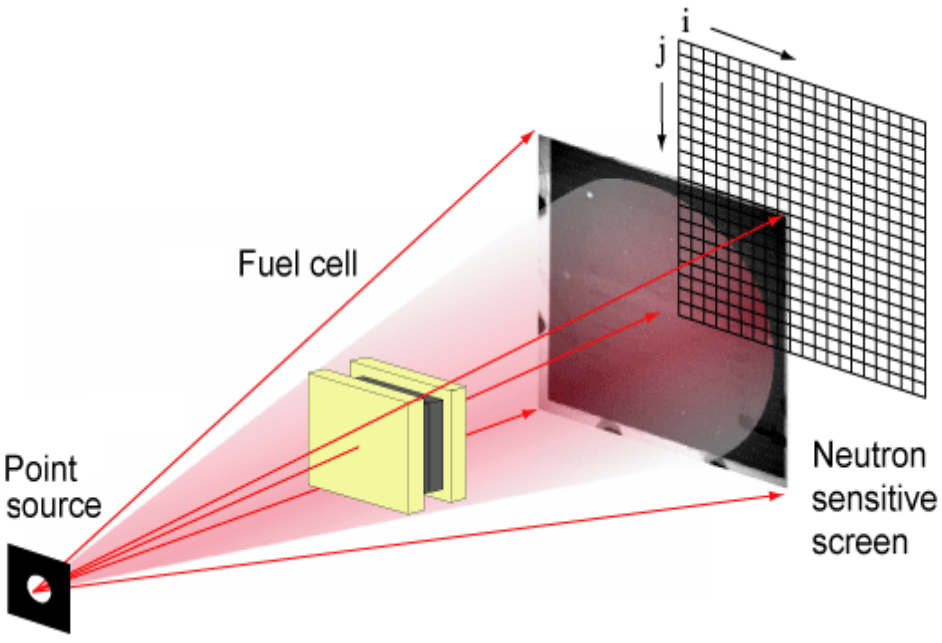

Figure. 1.3. Schematic of a standard neutron radiography system.

1.5.2. Principles of Neutron Tomography. Computerized tomography is a technique which can reconstruct the three dimensional image of the object from different radiographic images taken from different angles in small successive manner. These images can be mathematically manipulated to reconstruct a three dimensional image.One of the fastest and popular method of reconstruction is the filtered back projection algorithm (FBP)[16]. In this work FBP algorithm has been used to reconstruct neutron images. All projections are first arranged into a new set of images such that the $n'th$ pixel row of each projection is now stored sequentially in an individual image, also known as a sinogram. Every sinogram contains all the attenuation information for all possible angles. An implementation of inverse two dimensional Radon transform is then applied to calculate a cross sectional slice from each sinogram. Each reconstructed slice lies in a plane perpendicular to the axis of rotation. Collecting all slices into an image stack represents the three-dimensional attenuation distribution of the object. The image stack can be used to emphasis certain specific volume based on requirements.

The geometry of the imaging set up is influenced by the sample size and the pixel width (smallest possible scanning length or spatial resolution). The flux and the wavelength spread are directly related, the smaller the wavelength spread, the smaller the flux. This is also true for the spatial resolution; the smaller the pixel size (higher spatial resolution), the smaller the integrated flux at the pixel. Therefore, for attenuation based neutron imaging, full spectrum is used to get statistically significant results. For monochromatic imaging, generally (1-5%) $\Delta\lambda/\lambda$ is required to distinguish between materials. Scattering phenomena causes unwanted image artifacts in case of neutron radiography. They decrease the sharpness of the image. The disadvantage of neutron imaging over X-ray imaging is that

X-ray scattering cross section is regular and is related to the atomic number of the material being imaged, whereas neutron scattering cross sections are atomic number independent and statistical in nature. While that particular property makes neutron imaging suitable for locating light materials under heavy materials, it makes the elimination of scatter artifacts challenging.

For neutron radiography and tomography, collimators or slits are used to direct the radiation towards the object and get a point to point image. In order to obtain neutron image in a certain exposure time minimum number of neutron flux should be available. The exposure period is dependent on the problem and can vary from few second to several minutes. The exposure time and the neutron flux should be optimized together.

1.6. NEUTRON SOURCES AND FACILITIES

There are three main sources of neutrons; nuclear reactors, spallation neutron sources, and radioactive sources emitting neutrons. It might seem that it is not relevant where the neutrons are coming from, but neutron source spectrum has a massive impact on the imaging modality. The energy distribution of neutron source and background noise of the source (fast neutrons, gamma rays, delayed neutrons) can alter the quality of the image in a substantial way. They can also interact with the detector electronics. Therefore it is very important to choose which type of source to be used based on the requirement of the experiment. Nuclear reactors use fission to produce neutrons. Spallation neutron sources produce neutrons by hitting a target material with high energy protons. Both nuclear reactor and spallation source produce neutrons with the energy range of few mega electron volts.

However, in neutron imaging generally thermal or cold neutrons are used. A moderator must be used in order to slow down these fast neutrons. Neutrons can be produced from the radioactive sources, for example, Cf-252 isotope produce neutrons.

2. DETERMINISTIC SIMULATION METHOD

Neutron radiography is a useful tool for non-destructive imaging. There are several facilities across the world to conduct neutron imaging [18]. It is required to simulate the neutron images (radiographs) before actually doing the experiment to analyze the effectiveness of the imaging facility. Monte Carlo methods of simulation have been proven to be the most effective effective way to simulate the performance of a neutron imaging facility till date. However, Monte Carlo methods such as MCNP take a considerable amount of time to simulate a single radiograph. To form an image several radiographs are needed, therefore this method of simulation is proved to be extremely time consuming. It is true that with modern day parallel computation power, the image can be processed using multi-core computers [19]. This makes the computation procedure very costly. To make neutron imaging commercially effective, a faster and cheaper method needed to be developed. The other disadvantage of using stochastic methods to simulate images is that the uncertainty of the computation depends on the number of particles simulated. MCNP works on the basis of averaging a large number of particle histories over time. In nuclear imaging one principle concern is to reduce the dosage on the sample. Therefore, the less number of incident particles the less is the dose. Monte Carlo methods do not provide statistically significant results when there is less number of particle histories. In this present work, a deterministic method has been developed which solves both time and resource consumption problem. It is also effective way of simulating when there is less number of particles to be involved. This deterministic method is based ray tracing algorithm provided by the pioneer work of L. Siddon in 1985 [20]. This method assumes

neutrons as rays. Once the neutron ray passes through the subject and incident on the detector plane, this algorithm effectively tracks back (traces) each neutron ray which effectively and computes the path travelled within the sample to measure the attenuation. This work has been modified over the years by Freud et al, Zhao et al and Li at al [21-23]. This algorithm has a large application in the field of X-ray computed tomography. In this work the same principle has been applied to attenuation based neutron imaging. This deterministic approach consists of basic neutron attenuation law and ray-tracing techniques. A set of neutron rays are emitted towards the center of every pixel at the detector plane. Each ray passes through the object to be imaged. The object is divided into multiple voxels. Each ray passes through one voxel. The attenuation is calculated by measuring the length of the path each neutron ray covers within the object by determining the co-ordinates of the intersection points. The number of neutrons I(E), that emerge from the object and reaches the detector pixel is given by

$$I(E) = I_0 \Delta\Omega \exp(\textstyle\sum_i -\mu_i \, d_i) \tag{12}$$

Where, $\Delta\Omega$ is the solid angle through which neutron propagates, μ_i isneutron attenuation co-efficient of the $i'th$ voxel and d_i is the distance covered by the ray coming passing through the $i'th$ voxel. Based on the theory of neutron radiography, the attenuation of each ray is dependent on the path traversed by each ray inside the object. This object is most likely to be heterogenous. That means the neutron ray will traverse different path length within different materials. Identifying the path lengths travelled by each neutron ray within different material is very challenging. The entry and exit points of each neutron ray is calculated by measuring the dot product of direction vector of the ray line and the normal directed away from the object. Ray tracing determines all the intersections of a line or ray

from the source to the region of interest. From these intersections, the ray depth (d_i) can be calculated. The attenuation is given by $exp(-\mu_i d_i)$,where μ_i denotes the neutron attenuation co-efficient at the $i'th$ voxel.

In three dimensional Cartesian co-ordinate system, the ray is defined parametrically as a straight line connecting from point A to B.

$$X = X_A + \alpha(X_B - X_A)$$

$$Y = Y_A + \alpha(Y_B - Y_A)$$

$$Z = Z_A + \alpha(Z_B - Z_A)$$

The value of the parameter α is zero at point A and unity at point B. The plane curve is defined by the X-Z polygon. There are two conditions that the parameter α must satisfy to fulfil the ray-box intersection algorithm. The first condition is that Y co-ordinate of an intersection must lie on or within the Y extent of the object. The second condition is that all intersection points must lie between point A and B.

$$0 \leq \alpha \leq 1$$

2.1. PHYSICS MODEL

The physics model ray-tracing algorithm is given by the following equation:

$$I\ (\beta) = I_0(\beta)\exp(-\textstyle\sum_i \mu_i\, \rho_i d_i) + I_{sc}(\beta) + I_n(\beta) \qquad (13)$$

Where, $I(\beta)$ is the number of neutrons (or the neutron instensity) detected at the detector with source fan angle β, and $I_0(\beta)$ is the source intensity. β denotes the angular position of a ray in the neutron beam. μ_i, ρ_i, and d_i are respectively the mass attenuation coefficient, density, and path length of the ray which travels through the $i'th$ material. The sum extends over all the materials through which the neutron beam (ray) passes on the way to a

particular detector pixel. $I_{sc}(\beta)$ and $I_n(\beta)$ are the contributions to the detected neutron intensity from scattered neutrons and noise. Ray tracing algorithm only takes care of the uncollided neutron but in this work we have modified it so that it takes into account the effects of scattered neutrons and noise. The modified algorithm works in the following way:

1. Ray casting from the source to a particular pixel of the detector system.
2. Tracing the primary ray as it penetrates the object volume and calculating its attenuation.
3. Computing the scattered ray contribution with appropriate physics model and cross section.
4. Compute the statistical noise and scatter contribution with suitable physics models.
5. Accumulating the neutron intensity recorder by each detector pixel.

Steps 1-5 simulate neutron radiographic imaging. To simulate neutron tomography, the object volume is rotated to the next view angle and steps 1-5 are repeated.

For most common materials in NDT, the types of thermal neutron interaction are absorption, elastic scattering, and inelastic scattering. Microscopic cross section data for these interactions for different materials can be found in data libraries, such as ENDF/B-VII.1 [24]. In this work, a neutron mass attenuation coefficient data library was created for elements from hydrogen to zinc using the following equation:

$$\mu = \frac{N_A}{M}(\sigma_a + \sigma_s + \sigma_{in}) \tag{14}$$

Where, μ is the total mass attenuation coefficient, N_A is the Avogadro's number. M is the atomic mass. σ_a, σ_s, and σ_{in} are the absorption, elastic scattering, and inelastic

scattering microscopic cross sections, respectively. The calculation of the contributions of scattering and noise to the detected neutron intensity are described in the following sections.

2.2. NOISE MODEL

As with X-ray imaging, neutron imaging also suffers from inherent statistical noise. This noise is random and is generated due to effects like Poisson statistics on the detected number of neutrons, fluctuation of energy that each neutron deposits in the detector, and electronic readout noise, etc [25]. In this work, the neutron noise is modeled using a Poisson noise approximation. The neutron noise is estimated using a Poisson distribution, as shown in the following equation,

$$Pr(N = k) = exp(-\lambda t)\,(\lambda t)^k/k! \tag{15}$$

Where, N is the number of neutrons measured by a given detector element over a time interval t, and λ is the expected number of neutrons per unit time interval. The uncertainty described by this distribution is known as statistical noise. Because the incident neutron count follows Poisson distribution, it has the property that its variance is equal to its expectation as shown below:

$$E(N) = Var(N) = \lambda t \tag{16}$$

In the case of neutron imaging, the neutron noise is modeled as the Poisson noise σ (i.e., square root of the mean number of neutrons detected. Mathematically, it is expressed by the following equation:

$$\sigma(\beta) = \sqrt{I_0(\beta)\exp(-\textstyle\sum_i \mu_i\,\rho_i d_i)} \tag{17}$$

2.3. SCATTER MODEL

To simulate the contribution of scattered neutron to the detected density Kardijlov et al [26], Hassanein et al.[27], and later Hai-Feng and Bin[28] have defined a point scatter function by creating an image formed by a point source and a homogenous phantom using MCNP5. A scatter distribution function was developed which is dependent on the geometry of the phantom, and the fan beam angle of the source. The simulated data are processed with MATLAB [29] to form an analytic representation of the scatter distribution. The point scatter function depends on the size and shape of the object being imaged, as well as the distance between the object and the source. The main disadvantage of this method is that it is not a generalized method and needs a Monte Carlo simulation to be carried out to generate the scatter data.

In the present work, we have developed an approximate model of neutron scatter, which depends only on the incident intensity and the neutron intensity distribution over the detector. The foundation of this algorithm lies in the work of T.N.Hangartner[30], who formulated a forward scatter function for X-ray imaging, with later improvement of the work by Ohnesorge et al.[31]. The interactions between neutrons and matter create scattered rays in all possible directions.These rays, which can be either attenuated or scattered, create further cascaded scatter events. In neutron and X-ray imaging, first order scattering (where only one scatter interaction was included) accounted for the most severe image artifacts, since the first-order scatter contained the high frequency component of the scatter profile. This was due to the fact that non-uniformity of the object had a much stronger influence on the spatial distribution of the single scatter events than on the multiple scatter. For single scatter events, forward-scattered neutrons were most likely to penetrate

the object and reach the detector, due to a relatively shorter path length,as compared to the neutrons scattered in other directions. Multiple scattering in thermal neutron imaging is approximately a diffusion process, and results in a low frequency background.To account for both first-order and multiple scattering in neutron imaging simulation, the following assumptions are made:

1. The first-order scattering can be simulated by the forward scattering approximation described by the pioneering work of Hangartner and Ohnesorge et al.(1999).
2. Multiple scattering can be simulated using a convolution process, and the convolution kernel is a Gaussian function (i.e., a point spread function).

A schematic plot of the scatter model is shown in Figure. 3.1.The forward scatter intensity, $I_{sc,f}(\beta)$, coming from interactions between source neutrons (with fan angle β) and materials along the ray path, forms a point spread function at the detector. The total scatter distribution in a projection, $I_{sc}(\beta)$, results from superposition of scatter distributions from all source fan angles. Mathematically, it can be described as a convolution process, as shown in the following equation,

$$I_{sc}(\beta) = \int I_{sc,f}(\beta')G(\beta - \beta') = I_{sc,f}(\beta) \otimes G(\beta) \tag{18}$$

Where, $G(\beta)$ is a Gaussian function, and $\otimes$ represents the convolution operation.The forward-scatter can be approximately expressed by the following equation using MATLAB curve fitting tool[27].

$$I_{sc,f}(\beta) = K_{sc,f} I(\beta) \ln\left(\frac{I_0(\beta)}{I(\beta)}\right) \tag{19}$$

Where, $K_{sc,f}$ is a constant which is proportional to the scatter cross section of the materials along the ray path. In the present work, those constant are determined by benchmarking the scatter model against a MCNP5 simulation.

3. SIMULATION SETUP

The Monte Carlo simulation is considered to be one of the most accurate methods for simulating neutron transport due to its high fidelity physics model and its capability of handling complicated geometries. Parameters in the forward-scattering model and the Gaussian multiple scattering function are derived from Monte Carlo simulations performed using MCNP5(Figure.3.1) As shown in Figure.3.2a , a water cylinder that is 5cm high with a diameter of 5 cm is modeled as a uniform phantom. This uniform phantom can also be used for different cases by replacing water with a different type of material. An isotropic thermal neutron source with monoenergetic nergy of 0.0253ev and strength of $1x10^{11}$ neutrons/sec has been assumed so that the effect of inaccurate resonance cross sections can be ignored. Gadolinium is used to collimate the isotropic source.A neutron flux tally (FIR 5, Appendix A) has been used, which measures the normalized flux disrtribution in each detector pixel. The data are simulated separately for both uncollided and total (uncollided plus scattered) neutron contributions. The physics card 'NOTRN' has been used to find only the uncollided neutron distribution in the detector grid. The detector grid has a dimension of $10cm \times 10cm$.There are 100×100 pixels in the detector grid with pixel size equal to$1mm \times 1mm$. The distance between the center of the phantom to the source is 10 cm and the distance between the middle point of the detector grid to the center of the phantom is 5 cm. The scattered neutron distribution is obtained by subtracting uncollided neutrons from the total neutron contribution.As described in the next section, the scatter (including single and multiple scatter) effect ($I_{sc}(\beta)$) is modeled as a convolution process of forward scatter ($I_{sc,f}(\beta)$) with a Gaussian function G(β).

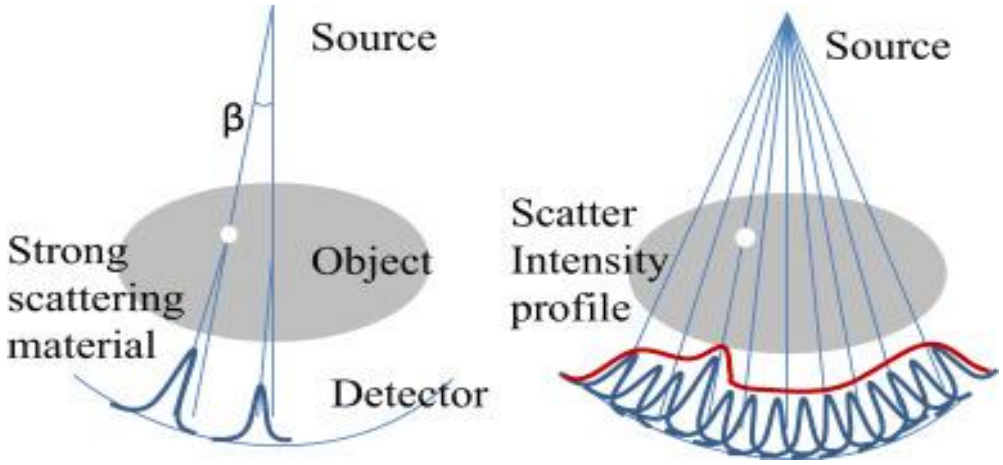

Figure.3.1. Schematic plot of the scatter model. Left: Forward-scatter and point spread function. Right: Convoluted overall scatter intensity profile.

The Gaussian function is estimated by comparing the results of the deterministic simulation and the MCNP5 simulation. To expand the scatter model to a more general case with heterogenous materials, the same deterministic methodology was used. Two simulation geometries were used. For the first one(referred to as geometry 1), a water cylinder (with the same dimensions as the previous homogenous water cylinder) was used with four smaller cylinders (1cm diameter each) filled with different materials inserts, including iron, lead, calcium, and air as shown in Figure.3.2b.As water is a highly scattering medium for thermal neutrons, the proposed simulation represented a very difficult problem for thermal neutron imaging. For the second simulation geometry (referred to as geometry 2 and shown in Figure.3.2c), an iron cylinder, with the same dimensions (height=5cm,diameter=5cm) was used; it was filled with four smaller cylinder of the same height and diameter(1cm each).The materials for these smaller cylinders were air,water,calcium,and lead respectively. Geometry 2 represented a thermal neutron

imaging case with a smaller scattering effect where iron (instead of water) was the main type of material in the phantom. The MCNP5 simulation was run for five million particle histories to obtain the uncollided and total neutron contributions, which resulted in less than 10% statistical uncertainties in the region of the phantom for all cases. Then, the scatter distribution was obtained by subtracting the uncollided neutrons from the scattered plus the uncollided neutron distribution. In the deterministic simulation, to account for the material non-uniformity, a modified scatter model was used:

$$I_{sc,f}(\beta) = K_{sc,f} I(\beta)^p ln\left(\frac{I_0(\beta)}{I(\beta)}\right)^q \tag{20}$$

Where, p and q are empirical constants.Tomographic simulation was performed using the deterministic method only, due to the excessively long computation time that would have been required using MCNP5.To obtain the tomographic reconstructed images, a series of 500 neutron radiography was simulated at different viewing angles with an angular increment of 0.72^0 using the deterministic method for both geometry 1 and geometry 2. The rotation period for geometry 1 and for geometry 2 are different due to the difference in neutron attenuation of these two geometries. The rotation time is 500 s per rotation for geometry 1 (due to high attenuation caused by water) and for geometry 2 it is 50 s per rotation. Three different cases were considered with the simulation:

(1) Simulation under ideal conditions(i.e. noiseless and no scatter contamination

(2) Poisson noise was added

(3) Both noise and scatter were added into the simulation.

Then the filtered back projection algorithm was used to reconstruct the tomographic images [32].

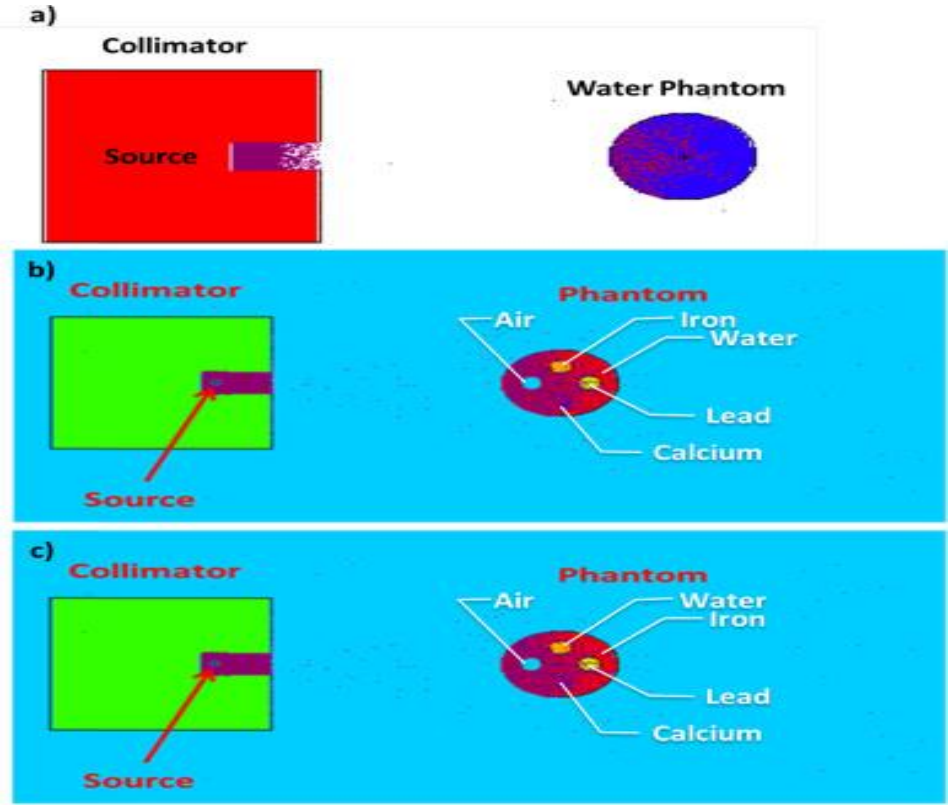

Figure.3.2. Simulation setup for different geometries. (a) A homogenous water phantom was irradiated by a collimated thermal neutron source. (b) Simulation geometry 1. (c) Simulation geometry 2.

4. RESULTS

First, the ideal 2D radiography images of the heterogenous phantoms(geometry 1 and 2) were simulated by both the Monte Carlo and the deterministic method; these included only the flux contributions of uncollided neutrons.The Monte Carlo simulations by MCNP5, using FIR5 tally are shown in Figure. 4.2a and Figure.4.3a. The deterministic simulations of the radiography at the same viewing angle are shown in Figure. 4.2b and Figure. 4.3b. The small cylinder inserts are clearly seen in all of the images. To quantitatively compare the Monte Carlo and deterministic simulations, a line profile comparisons are shown in Figure.4.2c and Figure.4.3c. The computation time for the deterministic simulation was significantly less than that for the Monte Carlo simulation.

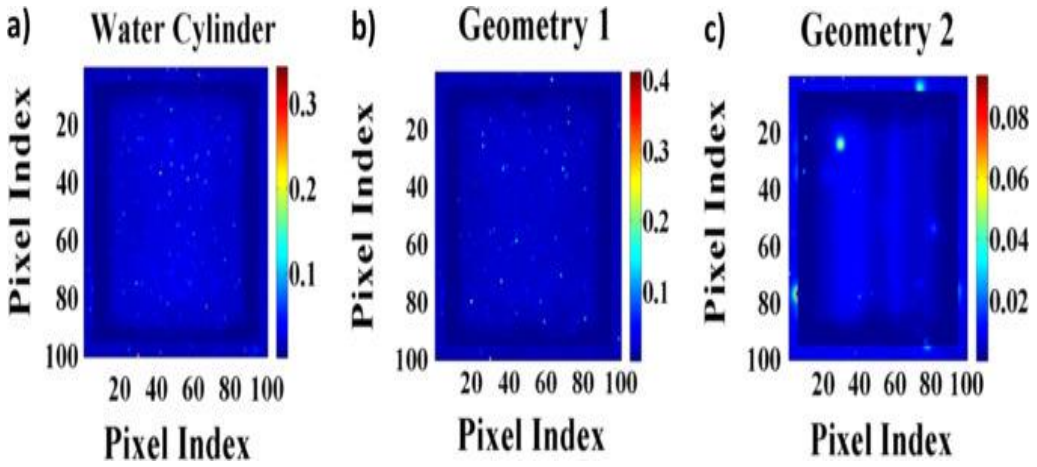

Figure. 4.1. Plot of statistical uncertainty of the MCNP simulations. The Colorbar represents the absolute value of the uncertainty.(a) Homogenous water cylinder. (b) Geometry 1. (c) Geometry 2.

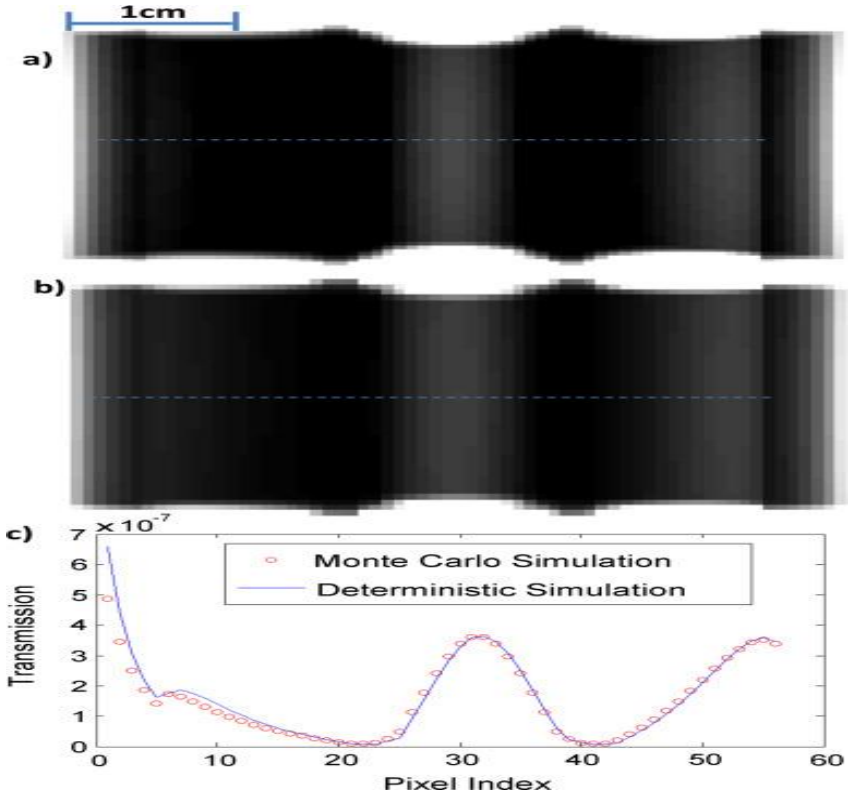

Figure.4.2. Simulated neutron radiography of geometry 1 under ideal conditions (i.e., noiseless and without scatter contamination) simulated by (a) Monte Carlo method. (b) Deterministic method. (c) Line profile comparison.

The next simulation shows the effect of the noise inserted into the simulated radiography images. As shown in Figure.4.4a, the ideal image is noiseless and without any scatter contamination. With the added Poisson noise, the deterministic simulated neutron radiography is shown in Figure.4.4b. The line profile comparison is shown in Figure.4.4c. To deterministically simulate the scatter effect, a Gaussian function was first estimated (shown in Figure.4.5). Using Eqs.18 and 20, the scattered intensity contributed to each pixel was calculated. In Eq.20, the parameters p and q were determined to be 0.18 and 1.0 respectively after many trials and errors respectively. . This pair of values worked out well

with different geometries. The value of $K_{sc,f}$ was strongly dependent on the major types of material in the simulated geometries.

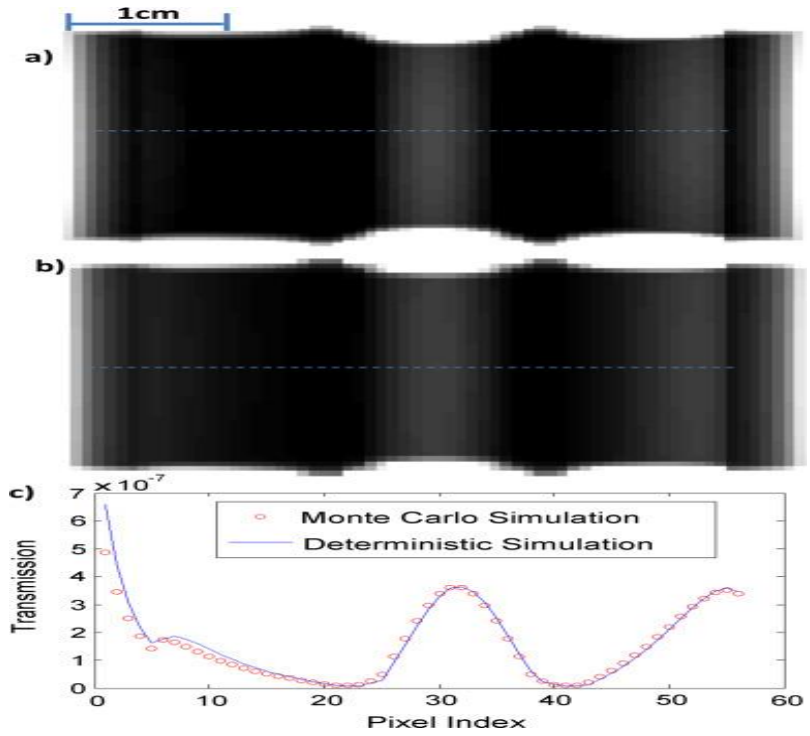

Figure.4.3. Simulated neutron radiography of geometry 2 under ideal conditions (i.e., noiseless and without scatter contamination) simulated by (a) Monte Carlo method. (b) Deterministic method. (c) Line profile comparison.

For geometry 1, $K_{sc,f}$ was strongly determined to be equal to 0.3, where water was the main type of material. The value of $K_{sc,f}$ was reduced to 0.03 for geometry 2, where iron was the main type of material. The deterministic simulations with added scatter were compared to the Monte Carlo simulations. The results are shown in Figures. 4.6 and 4.7.

The neutron radiography, with added scatter simulated by MCNP5 are show in Figures.4.6b and 4.7b. Because water is a material with a high elastic scattering cross section, the scattered neutron contribution was significant. The line profile comparison is shown in Figures.4.6c and 4.7c.

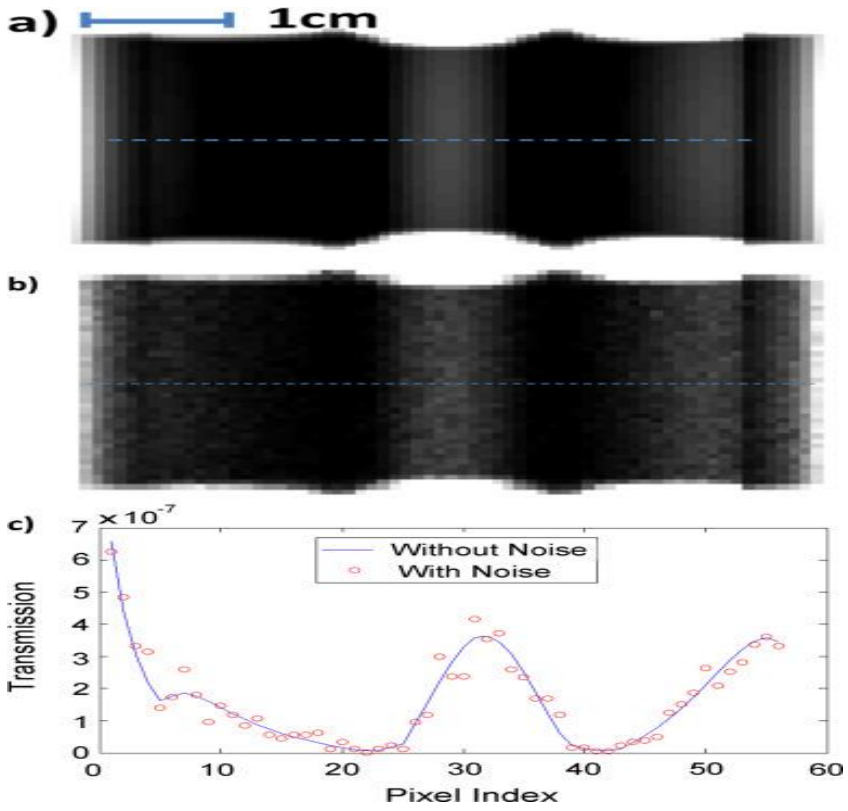

Figure.4.4. Neutron radiography of geometry 1. (a) Under ideal conditions (noiseless and without scatter contamination). (b) With added Poisson noise and without scatter contamination simulated by the deterministic method. (c) The line profile comparison.

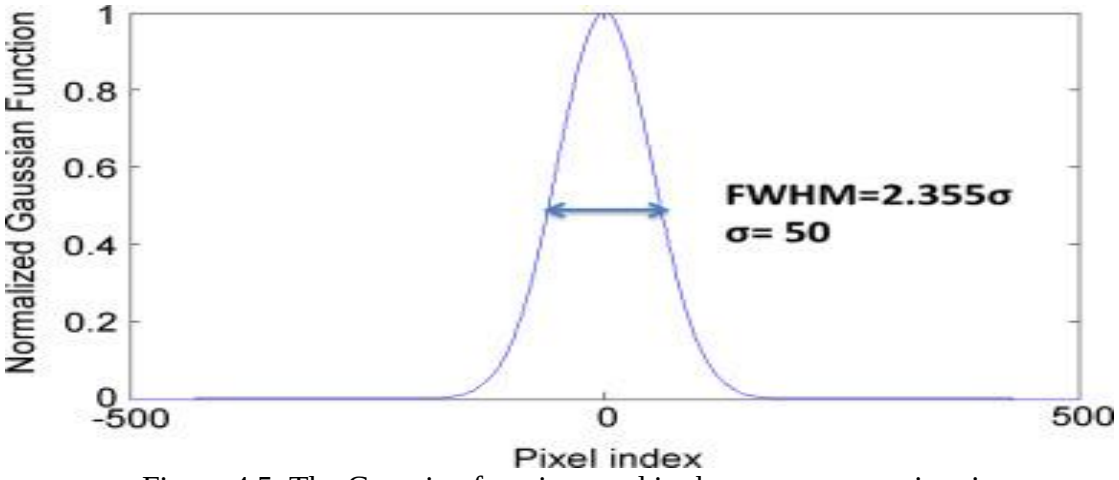

Figure.4.5. The Gaussian function used in the scatter approximation.

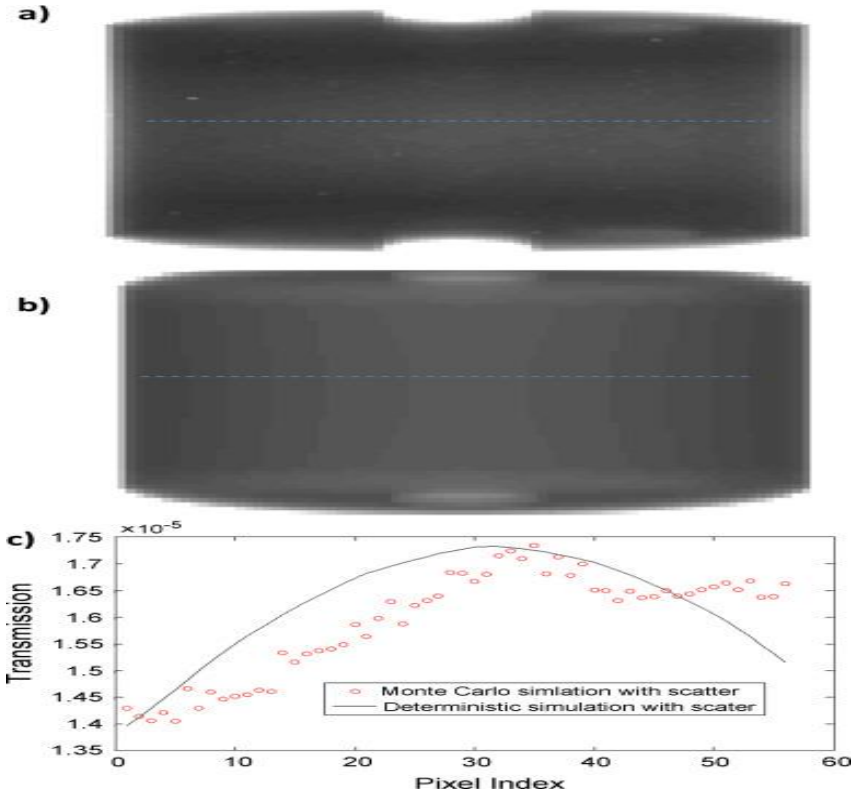

Figure.4.6. Neutron radiography of geometry 1. (a) With Scatter simulated by MCNP5. (b) With scatter simulated by the deterministic method. (c) Line profile comparison.

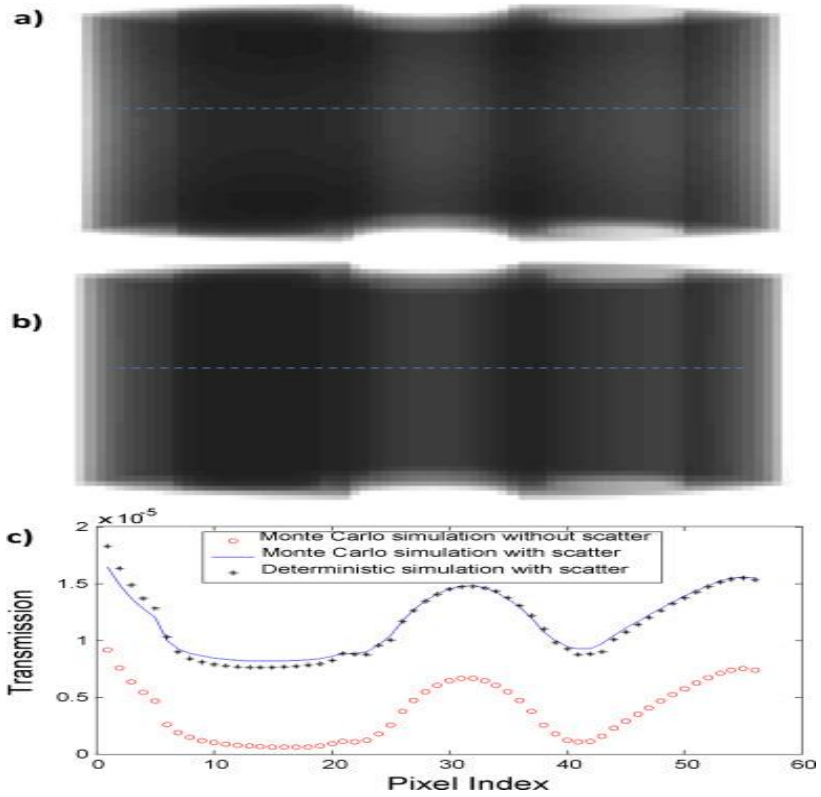

Figure.4.7. Neutron radiography of geometry 2. (a) With scatter simulated by MCNP5. (b) With scatter simulated by the deterministic method. (c) Line profile comparison.

As a comparison, the line profile of the Monte Carlo simulation without scatter is also plotted. Finally, the deterministic simulations of the neutron tomographic reconstruction are shown in Figures. 4.8. and 4.9. First, a tomographic image of geometry 1 and 2 under ideal imaging conditions (i.e. noiseless and without scatter contamination) are shown in Figures. 4.8a and 4.9a. The tomographic images (shown is Figures.4.8b and 4.9b) were reconstructed from neutron images with added Poisson noise. In Figures.4.8c and 4.9c, the tomographic images were reconstructed from neutron images with both added Poisson noise and scatter.

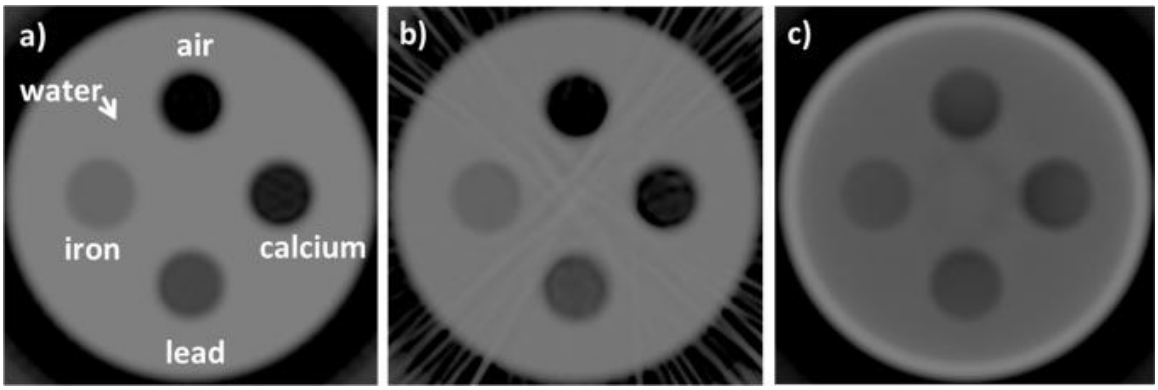

Figure.4.8. Tomographic image of geometry 1. (a) Under ideal conditions.
(a) With added Poisson noise. (c) With added noise and scatter.

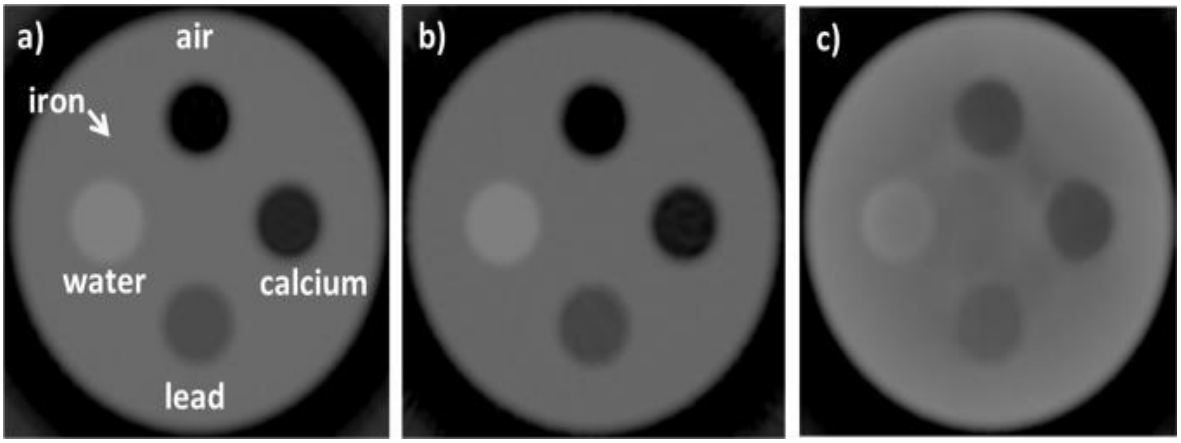

Figure. 4.9. Tomographic image of geometry 2. (a) Under ideal conditions.
(b) With added Poisson noise. (c) With added noise and scatter.

5. DISCUSSION

The deterministic method proposed in this paper can accurately simulate neutron radiography and tomography under ideal conditions (i.e., noiseless and without scatter contamination) with very efficient computation time. Simulation, with noise insertion, showed that a significant amount of noise can cause streak artifacts due to high attenuation of the material, as shown in Figure.4.8b.In a highly scattering hydrogenous medium, such as water, biological samples,etc., the scatter contamination is also significant, and must be corrected. Although scattering may reduce the noise effect as it increases the number of neutrons detected, it degrades the contrast significantly, and it also introduces a cupping artifact in the image (i.e., the dark region in the center of the image).

On the one hand, the scatter effect simulated by the deterministic method via forward scattering convoluted by a Gaussian broadening was generally in agreement with the results simulated by the Monte Carlo method for a highly scattering medium(e.g.,geometry 1). On the other hand, the deterministic simulations for a less scattering medium (e.g., geometry 2). The discrepancy in the simulated scatter effects between the deterministic and Monte Carlo methods in geometry 1 were mainly caused by the simplified scattering model, especially near the boundary of the phantom. The first-order scattering was simulated by a forward scatter model, and multiple scattering was simulated by a Gaussian convolution process. Three parameters ($p, q,$ and $K_{sc,f}$) control the distribution of scattered neutron intensity. The drawback of the proposed method is that the parameters are empirically determined by comparison with a Monte Carlo simulation. Parameter values used in the chosen heterogenous phantom may not be the ideal values for

an object or phantom with a significantly different material composition. However, the advantages if the proposed deterministic method outweigh the disadvantages. The computation time (usually a few seconds) is significantly less than that of Monte Carlo simulation. Therefore, it could be used in rapid prototype neutron imaging system design, image quality evaluation, etc. In addition, the empirical parameters were constant for imaging objects with similar material composition and dimensions. For some imaging, objects with different material composition but similar neutron interaction cross sections, it was expected that the empirical parameters would generate reasonable simulation results.

Due to significant scatter contamination in geometry 1, the tomographic reconstructed image (Figure.4.8c) was nearly useless the contrast of the four small cylinders was so low that they could hardly be recognized. For geometry 2, the scatter contamination was less significant as compared to the case of geometry 1. However, it was difficult to differentiate calcium from air, as shown in Figure.4.9c .Although the proposed modeling method for scatter effect can be useful in scatter correction, detailed analysis on scatter correction was beyond the scope of this work, and can be improved in future work.

6. CONCLUSION

The deterministic method presented in this work is very useful for fast simulation of neutron radiography and tomography. It can be used to design and optimize a neutron imaging system. Also, it is useful in developing scatter correction and noise removal algorithms to improve the quality of neutron imaging. Empirical parameters and the Gaussian function, which are dependent on materials, can be pre-determined for most materials with similar thermal neutron interaction cross section.

. **APPENDIX**

MCNP uses one tally called FIR5 which simulates an array of point detectors for planar radiograph flux image. The general representation of FIR5 is given as FIR5:N or FIR:P based on whether the incident particles are neutrons or photons, respectively. The unit of this tally is particles/sq.cm. The tally FIR establishes a flux image on a rectangular radiograph is given as below:

FIRn: pl X1 Y1 Z1 R0 X2 Y2 Z2 F1 F2 F3

n = The tally number ending with 5

pl=Particle type. N for neutrons and P for photons.

(X1, Y1, Z1) are the set of coordinates used with the entries on the Fsn and Cn cards to define the extent and spacing of the detector flux image grid. In the planar rectangular case (FIR), this point defines the center of the grid. R0 is not used here as the image grid was not out inside the scattering material. A zero has been placed to fill the place.

MCNP Code: Homogenous Water Phantom

CT Scanner Simulation

c

c ===== CELL DECK =====

c

c Phantom proper

```
10   9 -1.00 -10 -30 31 16 17 18 19 imp:n=1 imp:p=0   $ water

20   9 -1.00 -16 -30 31 imp:n=1 imp:p=0              $ calcium

30   9 -1 -17 -30 31 imp:n=1 imp:p=0               $ iron

40   9 -1.00000 -18 -30 31 imp:n=1 imp:p=0          $ air

50   9 -1.000 -19 -30 31 imp:n=1 imp:p=0            $ lead

c

c Collimators

101  4 -7.9 -101 102 imp:n=1 imp:p=0               $ Gadolinium

c

c Air surrounding system

900  3 -0.001205  -666 &

     #10 #20 #30 #40 #50 #101 imp:n=1 imp:p=0

c

1000 0 666 imp:n=0 imp:p=0   $ Void


c ===== SURF DECK =====

c

c Phantom surfaces

10 cz 2.500000    $ Phantom radius

30 pz 2.5    $ Front phantom surface

31 pz -2.50000    $ Back phantom surface

16 c/z 1.250000 0.00000 .5    $ Right hole

17 c/z -1.2500000 0.00000 0.5    $ Left hole
```

```
18 c/z 0.00000 1.250000 0.5   $ Top hole
19 c/z 0.00000 -1.2500000 0.5    $ Bottom hole
c
c
c Collimator Surfaces
101 RPP -10.00000 10.00000 8.00000 20.00000 -10.00 10.000 $ Outter collimator
boundary
102 RPP -0.60 0.60 8.00000 12.00000 -0.60 0.60   $ Inner collimator boundary
c
c
c Problem boundary
666 so 35.00000    $ Edge from beyond which there is no return

c ===== DATA DECK =====
mode n
SDEF ERG=2.53e-8 POS 0 10 0
c
c Steel
m1 &
     26000 1
c
c Air
m3 &
```

```
      6000 0.000150 &
7014 0.784431 &
8016 0.210748 &
 18000 0.004671
c
c Polyethylene
m2 &
     6012 0.495 &
     6013 0.005 &
     1001 0.5
c
c Collimator
m4 &
     64000 1.0000
m5 &
     82000 1.0000
c
c Polymethylmethacrylate (PMMA - C5O2H8)
m6 &
     6000 0.333345 &
     8000 0.133335 &
     1000 0.533320
c
```

```
c Calcium
m8 &
     20000 1.000
c
c Water
m9 &
     1001 0.666657 &
     8016 0.333343
FIR5:n 0 -5 0 0 0 10 0 0 0 0 $ radiography tally
FS5    -5 99i 5
C5     -5 99i 5
c notrn     $ only transmission
nps    5e6
prdmp 2j 1 1 j $ create a mctal file at the end of run
```

MCNP code for Geometry 1:

```
CT Scanner Simulation
c
c ===== CELL DECK =====
c
c Phantom proper
10   9 -1.00 -10 -30 31 16 17 18 19 imp:n=1 imp:p=0   $ water
20   8 -1.55 -16 -30 31 imp:n=1 imp:p=0              $ calcium
```

```
30   1 -7.87 -17 -30 31 imp:n=1 imp:p=0              $ iron

40   3 -0.001205 -18 -30 31 imp:n=1 imp:p=0          $ air

50   5 -11.34 -19 -30 31 imp:n=1 imp:p=0             $ lead

c

c Collimators

101  4 -7.9 -101 102 imp:n=1 imp:p=0                $ Gadolinium

c

c Air surrounding system

900  3 -0.001205  -666 &

     #10 #20 #30 #40 #50 #101 imp:n=1 imp:p=0

c

1000 0 666 imp:n=0 imp:p=0   $ Void


c ===== SURF DECK =====

c

c Phantom surfaces

10 cz 2.500000    $ Phantom radius

30 pz 2.5    $ Front phantom surface

31 pz -2.50000    $ Back phantom surface

16 c/z 1.250000 0.00000 .5    $ Right hole

17 c/z -1.2500000 0.00000 0.5    $ Left hole

18 c/z 0.00000 1.250000 0.5   $ Top hole

19 c/z 0.00000 -1.2500000 0.5    $ Bottom hole
```

```
c
c
c Collimator Surfaces
101 RPP -10.00000 10.00000 8.00000 20.00000 -10.00 10.000 $ Outter collimator
boundary
102 RPP -0.60 0.60 8.00000 12.00000 -0.60 0.60   $ Inner collimator boundary
c
c
c Problem boundary
666 so 35.00000    $ Edge from beyond which there is no return


c ===== DATA DECK =====
mode n
SDEF ERG=2.53e-8 POS 0 10 0
c
c Steel
m1 &
    26000 1
c
c Air
m3 &
     6000 0.000150 &
     7014 0.784431 &
```

```
      8016 0.210748 &
     18000 0.004671
c
c Polyethylene
m2 &
     6012 0.495 &
     6013 0.005 &
     1001 0.5
c
c Collimator
m4 &
     64000 1.0000
m5 &
     82000 1.0000
c
c Polymethylmethacrylate (PMMA - C5O2H8)
m6 &
     6000 0.333345 &
     8000 0.133335 &
     1000 0.533320
c
c Calcium
m8 &
```

```
     20000 1.000
c
c Water
m9 &
     1001 0.666657 &
     8016 0.333343
FIR5:n 0 -5 0 0 0 10 0 0 0 0 $ radiography tally
FS5   -5 99i 5
C5   -5 99i 5
c notrn  $ only transmission
nps    5e6
prdmp 2j 1 1 j $ create a mctal file at the end of run
```

MCNP code for Geometry 2:

```
CT Scanner Simulation
c
c ===== CELL DECK =====
c
c Phantom proper
10  1 -7.87 -10 -30 31 16 17 18 19 imp:n=1 imp:p=0   $ water
20   8 -1.55 -16 -30 31 imp:n=1 imp:p=0              $ calcium
30   9 -1.00 -17 -30 31 imp:n=1 imp:p=0              $ iron
40   3 -0.001205 -18 -30 31 imp:n=1 imp:p=0          $ air
50   5 -11.34 -19 -30 31 imp:n=1 imp:p=0             $ lead
```

```
c
c Collimators
101  4 -7.9 -101 102 imp:n=1 imp:p=0              $ Gadolinium
c
c Air surrounding system
900  3 -0.001205  -666 &
     #10 #20 #30 #40 #50 #101 imp:n=1 imp:p=0
c
1000 0 666 imp:n=0 imp:p=0   $ Void


c ===== SURF DECK =====
c
c Phantom surfaces
10 cz 2.500000    $ Phantom radius
30 pz 2.5    $ Front phantom surface
31 pz -2.50000    $ Back phantom surface
16 c/z 1.250000 0.00000 .5    $ Right hole
17 c/z -1.2500000 0.00000 0.5    $ Left hole
18 c/z 0.00000 1.250000 0.5   $ Top hole
19 c/z 0.00000 -1.2500000 0.5    $ Bottom hole
c
c
c Collimator Surfaces
```

```
101 RPP -10.00000 10.00000 8.00000 20.00000 -10.00 10.000 $ Outter collimator
boundary
102 RPP -0.60 0.60 8.00000 12.00000 -0.60 0.60   $ Inner collimator boundary
c
c
c Problem boundary
666 so 35.00000    $ Edge from beyond which there is no return


c ===== DATA DECK =====
mode n
SDEF ERG=2.53e-8 POS 0 10 0
c
c Steel
m1 &
    26000 1
c
c Air
m3 &
     6000 0.000150 &
     7014 0.784431 &
     8016 0.210748 &
    18000 0.004671
c
```

```
c Polyethylene
m2 &
    6012 0.495 &
    6013 0.005 &
    1001 0.5
c
c Collimator
m4 &
    64000 1.0000
m5 &
    82000 1.0000
c
c Polymethylmethacrylate (PMMA - C5O2H8)
m6 &
    6000 0.333345 &
    8000 0.133335 &
    1000 0.533320
c
c Calcium
m8 &
    20000 1.000
c
c Water
```

```
m9 &
    1001 0.666657 &
    8016 0.333343
FIR5:n 0 -5 0 0 0 10 0 0 0 0 $ radiography tally
FS5   -5 99i 5
C5   -5 99i 5
c notrn  $ only transmission
nps    5e6
prdmp 2j 1 1 j $ create a mctal file at the end of run
```

BIBILOGRAPHY

[1] H. Berger, F. Iddings, "Neutron Radiography - a State-of-the-Art Report." Nondestructive Testing Information Analysis Center, NTIAC-SR-98-01, Austin TX-1998.

[2] F.Fiori, G.Giunta, A. Hilger ,N.Kardijlov, F.Rustichelli.(2006,Nov) "Non-destructive characterization of archaeological glasses by neutron tomography."Physica B:Condensed Matter.Vol. 385-386(2), pp.1206-1208.

[3] J. J.Boo.et al.,(2015). "Neutron radiography for the study of water uptake in painting canvases and preparation layers." Appl.Phys.A.

[4] E.Craft. et al. (2014.Oct). "Neutron radiography of irradiated nuclear fuel at Idaho National Laboratory".PhysicsProcedia.Vol.69,pp. 483-490. Available: http://dx.doi.org/10.1016/j.phpro.2015.07.068.

[5] N.Putra, R.S.Ramadhan, W.N.Septiadi, Sutiarso. (2015 Sep). "Visualization of boiling phenomena inside a heat pipe using neutron radiography." Experimental thermal and fluid science.Vol.66, pp. 13-27. Available: http://dx.doi.org/10.1016/j.expthermflusci.2015.02.026.

[6] M. Tharwat, N. Mohamed, T. Mongy. (2014, Feb.). "Image enhancement using MCNP5 code and MATLAB in neutron radiography." Applied Radiation and Isotopes.Vol. 89, pp.30-36. Available: http://www.ncbi.nlm.nih.gov/pubmed/24583508.

[7] J. Chadwick .(1932). "Possible Existence of a Neutron." Nature.Vol.129, pp.312.

[8] Y. Segal, Gutman, A. Fishman, A. Notea. (1982) "Point spread function due to neutron scattering in thermal neutron radiography of aluminum, iron, zircon, and polyethylene objects. Nuclear Instrumentation and Methods., Vol.197.pp. 557.

[9] Y.Murata., et al. (1992). "Two-dimensional neutron image excluding the effect of scattered neutrons." Vol. 4. Gordon and Breach Science Publications, pp. 583–590.

[10] D.A. Raine, J.S. Brenizer. (1996,June). "A scattering effect correction for high resolution neutron radiography and computed tomography." in: Fifth World Conference on Neutron Radiography, Berlin, pp.17–20.

[11] N.Kardijlov. et al. (2003). "Further developments and applications of radiography and tomography with thermal and cold neutrons."Ph.D dissertation, Technische Universität München, Fakultät für Physik, 2003.

[12] Liu .Shu-Quan., et al., 2013. " Corrections on energy spectrum and scatterings for fast neutron radiography at NECTAR facility." Chinese. Physics. C .Vol.37 (11). pp.81-70.

[13] Chankow, Nares, 2012. Neutron Radiography, Nondestructive Testing Methods and New Applications. In: Omar, Mohammad (Ed.), InTech. ISBN: 978-953-51-0108- 6.

[14] G.N .Hounsfield (1973) "Computerized transverse axial scanning (tomography)." Part 1. Description of system. Br J Radiol 46:1016–1022.

[15] W.R.Madych. (2004,Nov). "Radon's Inversion Formulas." Transactions of the American Mathematical Society.Vol.356 (11), pp.4475-4491.

[17] J. Chadwick .(1932). "Possible Existence of a Neutron." Nature.Vol.129, 312.

[18] A.K .Heller.,J.S,Brenizer.,2010. " NeutronRadiography.In:Anderson,I.,etal.(Eds.), Neutron Imaging and Applications:AReferencefortheImagingCommunity." Springer,NY,pp.67–80.

[19] R.B.M .Sogbadji.,et al.,(2014). "The design of a multi source americium–beryllium (Am–Be) neutron irradiation facility using MCNP for the neutronic performance calculation." App.Radiat.Isot. Vol.90,pp.192–196.

[20] R.L.Siddon., 1985. "Prism representation:a 3D ray-tracing algorithm for radio-therapy applications."Phys.Med.Biol. Vol.30(8), pp.817–824.

[21] N.Freud. et al.(2004). " Deterministic Simulation of First-Order Scattering in Virtual X-ray Imaging." Nuclear Instrumentation Methods.Phys.Res.B .Vol.222(1-2), pp.285-300.

[22] H.-X.Zhao, et al.(2007). "Afastalgorithmforvoxel-baseddeterministicsimulation of X-Ray imaging." Comput.Phys.Commun.Vol.178(7), pp.518–523, Available: http:// dx.doi.org/10.1016/j.cpc.2007.11.008.

[23] N.Li.,et al.,(2007). "Virtual X-ray imaging techniques in an immersive casting si-mulation environment." Nucl.Instrum.Methods.Phys.Res.B .Vol.262(1),pp.143–152.

[24] M.B.Chadwick.,et al.,2011. "ENDF/B-VII.1:Nuclear data for science and technology: cross sections,covariances, fission product yield and decay data.Nucl.Data Sheets 112(12),pp.2887–2996.

[25] R.Lewandowski, L.Cao.,D.Turkoglu.,(2012). "Noise evaluation of a digital neutron imaging device." Nucl.Instrum.Methods Phys.Res. A. Vol.674,pp. 46–50.

[26] N. Kardijlov., et al.,(2005). “Scattering Corrections in Neutron Radiography using point scattered functions.” Presented at ITMNR-5.

[27] R.Hassanein., F.C .DeBeer.N.Kardijlov., E.Lehmann., (2006). “Scattering correction algorithm for neutron radiography and tomography tested at facilities with different beam characteristics.”Phys.B:Condens.Matter. Vol.385–386 (2), pp.1194–1196.

[28] H-F.Dou.,B.Tang.,2011. “An empirical formula for scattered neutron components in fast neutron radiography.”Chin.Phys.C. Vol.35(5),pp.483–487.

[29] MATLAB and Statistics Toolbox Release 2012, The MathWorks, Inc., Natick, Massachusetts, United States.

[30] T.N.Hangartner.(1987). “Correction of scatter in computed tomography images of bone.” Med.Phys.Vol.14(3),pp.335–340.

[31] B.Ohnesorge.,et al.,(1999). “Efficient object scatter correction algorithm for third and fourth generation CTscanners.”Eur.Radiol.Vol.9(3),pp.563–569.

[32] A. C. Kak and Malcolm Slaney,“Principles of Computerized Tomographic Imaging” IEEE Press, 1988.

VITA

Rajarshi Pal Chowdhury was born in Kolkata, India. He received his Bachelor of Technology (B.Tech) degree in Electronics and Communication Engineering from West Bengal University of Technology in July, 2006. He received his Master of Technology (M.Tech) from Indian Institute of Technology, Kanpur in the major Nuclear Engineering &Technology Programme in Aug, 2013. Rajarshi Pal Chowdhury received his MS degree from Missouri University of Science and Technology in the major Nuclear Engineering in July, 2016. His master's thesis was in the topic "Deterministic Simulation of Thermal Neutron Radiography and Tomography." He, along with his advisor Dr. Xin Liu published a journal article with the same name in the peer-reviewed journal "Radiation Physics & Chemistry".